Electrochimica Acta 228 (2017) 91–99

Contents lists available at ScienceDirect

Electrochimica Acta

journal homepage: www.elsevier.com/locate/electacta

Carbon-free Solid Dispersion $LiCoO_2$ Redox Couple Characterization and Electrochemical Evaluation for All Solid Dispersion Redox Flow Batteries

Zhaoxiang Qi, Aaron L. Liu, Gary M. Koenig Jr*

Department of Chemical Engineering, University of Virginia, 102 Engineers Way, Charlottesville, VA, 22904-4741, USA

ARTICLE INFO

Article history:
Received 5 September 2016
Received in revised form 9 January 2017
Accepted 10 January 2017
Available online 11 January 2017

Keywords:
flow battery
lithium cobalt oxide
lithium-ion
suspension
viscosity

ABSTRACT

Semi-solid flow batteries have been reported to have among the highest energy densities for redox flow batteries, however, they rely on percolated carbon networks which increase the electrolyte viscosity significantly. We report the first demonstration of carbon-free redox flow couples comprised of dispersed lithium-ion battery active material suspensions, with sub-micrometer $LiCoO_2$ (LCO) particles at the cathode and $Li_4Ti_5O_{12}$ (LTO) particles at the anode. Both electrochemical and rheological properties of the LCO suspensions are reported and compared to previous reports for LTO dispersed electrochemical redox couples. An LTO anode and LCO cathode full cell was constructed and reversible electrochemical redox reaction of the dispersed particles was successfully demonstrated. This carbon-free dispersed lithium-ion active material full cell provides a proof-of-concept for a system that lies between the relatively high viscosity semi-solid flow cells with percolated carbon networks and the relatively low energy density conventional flow cells comprised of dissolved transition metals, providing a system for future study of the trade-off between energy density and viscosity for electrochemical flow cells that rely on solid active materials.

1. Introduction

Redox flow batteries provide the flexibility to independently design the power and energy for applications by separating energy storage via electrolyte storage tanks and the power output in the electrochemical reaction cells [1,2]. This is important for large-scale applications, and stationary flow battery technology has been commercially demonstrated in kW and even MW scales in recent years [3,4]. One challenge for many flow batteries is that the solubility of the active species in the electrolyte is limiting the energy density due to formation of inactive precipitates at high concentrations [3,5,6]. Various efforts have been explored to increase the energy density, for example, polymer based flow batteries [7–10], new active materials [11,12], ionic liquids [13], and hybrid flow batteries with multiple redox couples [14]. Another recently explored redox flow battery, so-called semi-solid flow battery, bypasses the limitation of active material solubility on energy density by starting with solid active material particles in the electrolyte. This technology is promising because it provides significant improvements in energy density and also uses lithium-ion active materials, which results in a high operating voltage [15,16]. However, the high viscosity of the carbon-percolated electrolyte in these systems is a challenge due to the relatively high parasitic energy required to pump the semi-solid electrolyte [16,17]. Recently, our group reported initial results for a system that lies between conventional flow batteries (relatively low viscosity and energy density) and semi-solid flow batteries (relatively high viscosity and energy density) by dispersing a lithium-ion battery active material within an electrolyte and reversibly electrochemically oxidizing and reducing the active material particles during collisions with a current collector in the suspension [18]. Relatively low viscosities are achieved by not adding carbon to form a percolated network in the system while theoretically high energy density is maintained by starting with solid electroactive materials. This previous initial report of what was termed a

* Corresponding author at: Department of Chemical Engineering, University of Virginia, 102 Engineers Way, Charlottesville, VA, USA, 22904–4741, Tel.:+ 1 434 982 2714, fax: +1 434 982 2658.
E-mail address: gary.koenig@virginia.edu (G.M. Koenig).

http://dx.doi.org/10.1016/j.electacta.2017.01.061
0013-4686/

"dispersion flow battery" redox couple was a half-cell demonstration that paired a lithium metal anode with a target anolyte material dispersion containing $Li_4Ti_5O_{12}$ (LTO) active material. However, a target catholyte material for a carbon-free solid dispersion flow battery has previously not been reported, nor has a reversible full cell comprised of only dispersed lithium-ion active material particles for both the anode and cathode reactions.

Herein, we detail the first report of a carbon-free solid dispersion flow battery target catholyte material by using $LiCoO_2$ (LCO) as a redox couple. LCO was chosen as the target cathode material for a solid dispersion flow redox couple because of its relatively high electronic and ionic conductivities relative to other common lithium-ion cathode materials [19]. High ionic and electronic conductivity are necessary such that ambipolar diffusion is sufficient to not result in a prohibitive resistance in the collision electrochemical environment without carbon additives in a supporting electrode [18,20]. LCO's conductivity has previously been reported to be sufficient to provide full charge/discharge cycles of thick carbon-free pellet electrodes, suggesting charge and discharge of LCO particles in contact with a current collector while dispersed into an electrolyte should be possible [21]. LCO is also one of the most widely used cathode materials and both structural and electrochemical properties have been reported in the literature [22–27]. LCO has a discharge voltage of ~4.0 V vs. Li/Li^+ and a high energy density [28,29].

We also report the first demonstration of an electrochemical dispersion cell comprised exclusively of solid dispersions of electroactive lithium-ion battery particles by pairing carbon-free solid dispersions of a catholyte containing LCO and an anolyte containing LTO. A full cell with LCO as the cathode and LTO as the anode in a conventional static lithium-ion battery cell has previously been reported to have a stable ~2.5 V cell voltage [30], which would be significantly greater than the average discharge voltage of common conventional flow batteries such as vanadium-containing systems [31]. While the power density of the initial electrochemical cell in this report is very low, the theoretical capacity and cell voltage of a solid dispersion electrochemical cell with LTO and LCO shows promise in flow-based electrochemical energy storage applications.

2. Experimental

2.1. Preparation and Characterization of LCO and LTO Materials

The synthesis of LCO was described in detail in a previous report [32]. In brief, $CoC_2O_4{\cdot}2H_2O$ precursor was synthesized via a co-precipitation method. Equal volume of 0.1 M $(NH_4)_2C_2O_4$ and 0.1 M $Co(NO_3)_2$ solutions were mixed at 60 °C to form $CoC_2O_4{\cdot}2H_2O$. The solid particle precipitates were dried at 80 °C before being mixed with LiOH and calcined in a Carbolite CWF 1300 box furnace in an air atmosphere. The mixture was fired to 800 °C at a rate of 1 °C/min before turning off the furnace and allowing cooling to ambient temperature. The LCO product was milled to smaller particles through a wet soft milling procedure on a roller (US Stoneware) with zirconia beads.

LTO (NEI Corporation) powders were used as delivered. The characterization of the LTO material from NEI has been reported previously by our group and others [18,33,34]. The electrolyte (BASF Corporation) in the LCO suspensions and all electrochemical tests was 1.2 M lithium hexafluorophosphate ($LiPF_6$) in ethylene carbonate (EC) and ethyl methyl carbonate (EMC) with EC:EMC = 3:7 by volume ratio. The LCO suspensions of different loadings (0.5 vol%, 5 vol%, 10 vol%, 20 vol%) were prepared by mixing LCO powders with electrolyte under stirring overnight within an argon-filled glove box (with concentrations of $O_2 < 1$ ppm and $H_2O < 1$ ppm) at room temperature. The LTO suspension was prepared in the same way. Rheological characterization of the LCO suspensions were performed with an Anton Paar rheometer (Physica MCR 301, with a 5 cm plate-plate geometry). Scanning electron micrograph (SEM) images were taken for both LCO and LTO with a Quanta 650 SEM.

2.2. Electrochemical Testing

2.2.1. Conventional Coin Cell Fabrication

Electrochemical characterization was done by using CR2032 type coin cells with the LCO electrode as the cathode and lithium foil as the anode for half-cell tests and an LTO electrode as the anode for full cell tests. The electrodes were separated by a polypropylene/polyethylene/polypropylene trilayer membrane. LCO or LTO electrodes used in coin cells were fabricated from slurries comprised of 80 wt % LCO or LTO powder, 10 wt % carbon black as conductive additive, and 10 wt % polyvinylidene fluoride binder (PVDF) dissolved in N-methylpyrrolidone (NMP, Sigma-Aldrich®). The slurry was agitated in a slurry mixer for 5 minutes and pasted (with a doctor blade) onto aluminum foil. The pasted slurry was dried in an oven at 70 °C overnight and further dried in a vacuum oven at 70 °C for 3 h.

2.2.2. Particle Coin Cell Fabrication

Electrodes composed of only LCO particles as the electrode material without binders or conductive additives on the aluminum foil were prepared. LCO particles were suspended in acetone (Fisher Scientific), dropped on pre-punched aluminum foil discs

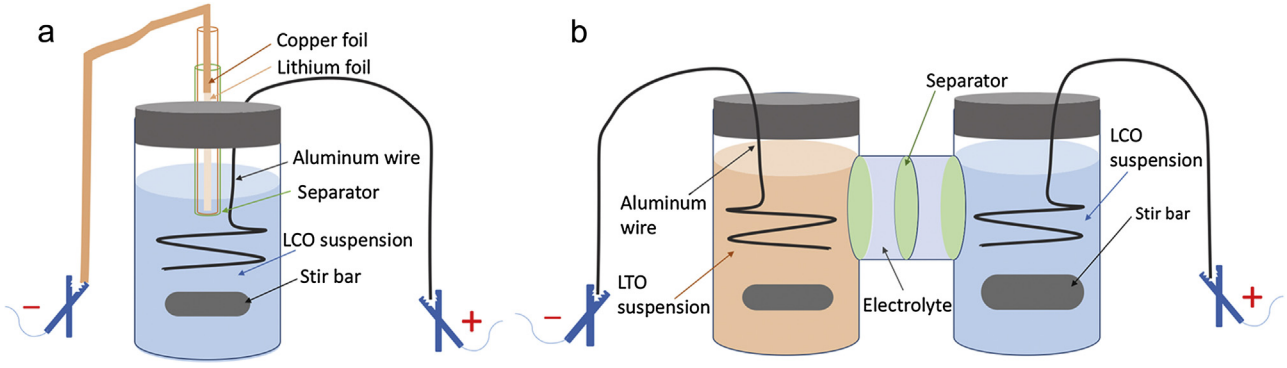

Fig. 1. Schematic of cell configurations: (a) a vial cell with the aluminum wire in the LCO suspension as the cathode current collector and lithium foil in a glass tube as the anode; (b) a full cell with aluminum wires in the LCO suspension as the cathode current collector and in the LTO suspension as the anode current collector.

(1.6 cm^2), and then dried in a vacuum oven at 70 °C for 2 h. A coin cell using the as-prepared electrode was referred to as a "particle coin cell".

2.2.3. Conventional and Particle Coin Cell Electrochemical Characterization

All coin cells were assembled in the glove box. The galvanostatic charge-discharge cycling of coin cells was performed on a Maccor battery cycler. For all cycling tests where C rates are given, 1C was assumed to be 180 mA g^{-1} with the mass being the mass of LCO and the current was adjusted by the amount of LCO active material in the electrode.

2.2.4. Active Material Suspension Characterization in Customized Cells

A customized cell (referred to as a "vial cell") as illustrated in Fig. 1a was set up in the glove box to perform half-cell tests. An aluminum wire (9.4 cm^2, Alfa Aesar) was immersed in an LCO suspension of a desired particle loading. Lithium foil, which was attached to a copper foil extended to the external circuit, was immersed into the electrolyte within a glass tube and separated from the LCO suspension by a trilayer membrane separator. A potentiostat (Bio-Logic, SP-150) was used to perform electrochemical tests while the suspension was agitated by stirring.

Another customized cell was set up in the glove box to perform full cell tests as illustrated in Fig. 1b. An aluminum wire (14.1 cm^2, Alfa Aesar) was immersed in a 0.5 vol% LCO suspension and another one in a 1 vol% LTO suspension. The two electrodes were separated by three polypropylene/polyethylene/polypropylene trilayer membranes to prevent active material crossover. The potentiostat was used to perform electrochemical tests while both suspensions were agitated by stirring.

3. Results and Discussions

3.1. Electrochemical Characterization of the LCO Coin Cells

We adopted a synthesis method to produce sub-micrometer sized LCO material that had been previously reported [32], because sub-micrometer sized or nano-sized particles are needed to form stable suspensions in the electrolyte and we were not able to obtain suitable sized commercial LCO materials. Fig. 2a displays typical charge/discharge profiles for the first 4 cycles of a Li/LCO cell with the LCO distributed within a conventional composite electrode. The voltage window for the cell was 2.5 – 4.5 V and the charge/discharge rate was 0.1C. The voltage profile was consistent with previous reports on LCO materials [22,28,29,35–39]. The first charge capacity reached 196 mAh g^{-1} with a discharge capacity of 171 mAh g^{-1}. We attribute the loss of capacity during the first cycle to both SEI formation and electrolyte decomposition at the relatively high cutoff voltage [40–42]. Subsequent cycles after the first charge/discharge had coulombic efficiency of >95%.

Two key differences between electrochemical oxidation/reduction of LCO particles in a conventional lithium-ion battery composite electrode compared to dispersion of the active material particles in a flowing electrolyte are that 1) the dispersion system does not contain conductive carbon additives and binder materials and 2) due to the active material being dispersed in the electrolyte only the LCO material in contact with the current collector at any given time participates in the electrochemical reaction. Therefore, we fabricated particle coin cells described in the Experimental section to confirm the electrochemical activity of the LCO material directly deposited on the current collector and in the absence of binders and conductive additives, which is more similar to the environment the LCO material will experience in the custom flow cells. The first 4 charge/discharge profiles for a Li/LCO particle coin cell using the same C rate and voltage window as the conventional LCO electrode coin cell are shown in Fig. 2b. The initial charge capacity was 179 mAh/g, while the discharge capacity was 140 mAh/g. The overall capacity was lower than the conventional coin cell and only 78% capacity was retained for discharge in the first cycle. The capacity on following cycles dropped significantly and only 42% of the discharge capacity was retained after only four cycles at 0.1C. We attribute the loss in discharge capacity to the volume change of LCO particles during cycling, which caused disconnection of loosely packed LCO particles from the current collector, resulting in a loss of capacity [43]. Particle coin cells containing LTO retain a much greater fraction of initial discharge capacity with cycling at low rates of charge/discharge (see [18] and Fig. S1 in the Supplementary Materials) compared to the LCO material. LTO has been reported to be a zero-strain material that does not undergo volume change during cycling, while LCO has been reported to have volume changes of ~2.3% during charge/discharge [44–46]. We thus suspect the strain from the volume change of the LCO material accelerates the disconnection of

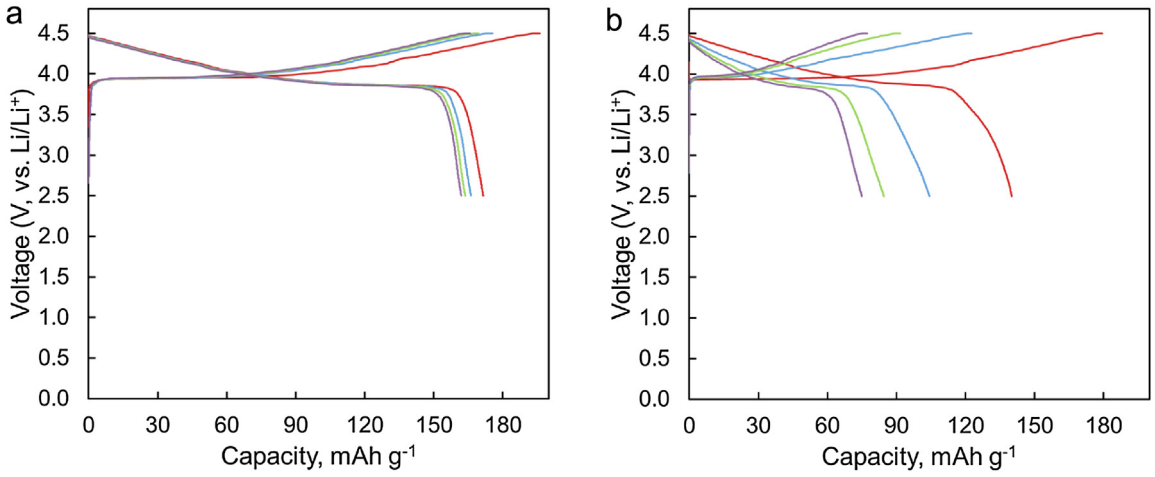

Fig. 2. Charge/discharge profiles for cycles 1 (red), 2 (blue), 3 (green), and 4 (purple) for (a) a LCO conventional coin cell and (b) a LCO particle coin cell, both charged/discharged at a rate of 0.1C between a voltage window of 2.5 to 4.5 V.(For interpretation of the references to color in this figure legend, the reader is referred to the web version of this article.)

material from the current collector due to mechanical forces accompanying the particle strain and accelerates the fade in the discharge capacity for LCO particle coin cells relative to LTO. However, the initial charge capacity for the LCO particle coin cell was close to that observed for the conventional LCO coin cell and the potential for lithium extraction and insertion was not significantly impacted, suggesting that the LCO particles can be successfully charged and discharged without conductive carbon additives or binders. Thus, these results provided motivation and support that a dispersion of LCO particles could be effectively charged and discharged through direct contact of LCO particles with the current collector during collisions within a flowing suspension.

3.2. Rheological Characterization

Before studying the electrochemical properties of the LCO suspensions, the rheological properties of the LCO particles dispersed in the electrolyte were investigated, and also were compared to the rheological data reported for similar suspensions containing LTO particles [18]. The viscosities as a function of shear rate for LCO can be found in Fig. S2 in the Supplementary Materials. Both the particle-free and particle-laden electrolytes show shear-thinning behavior, with the viscosity increasing as the particle volume fraction is increased across all measured shear rates. From these data for LCO suspensions and previous data for LTO suspensions [18], we have extracted the viscosity and relative viscosity (the suspension viscosity divided by the carrier electrolyte viscosity) as a function of particle volume fraction at a shear rate of $100\,s^{-1}$ (Fig. 3). For equivalent volume fractions, the viscosities of both the LCO and LTO suspensions are very similar. This is consistent with the similar approximate sizes and morphologies for both of the suspensions (360 ± 140 nm for LCO and 340 ± 200 nm for LTO, representative SEM images can be found in Fig. S3 in Supplementary Materials) [18,32]. Particle size has previously been reported to have significant influence on rheological properties of solid suspensions [47,48], where suspensions with smaller solid particles generally have measured higher viscosities [48,49]. The viscosity of metal oxide suspensions are also dependent on the volume fraction of solid particles loaded in the dispersion and can be modeled by the relationship in Equation 1 [50,51].

$$\eta = ae^{b\phi} \tag{1}$$

where η is the viscosity of the suspension, ϕ is the volumetric solid particle loading, and a and b are fitting parameters. The parameter b indicates the viscosity's exponential dependence on volumetric loading. A higher b means a stronger exponential relationship with ϕ. With the extracted viscosity data for LCO and LTO at different particle loadings, we can fit the data in Fig. 3 to this power law relationship to extract the a and b parameters (the fit curves are shown in Fig. S4 in the Supplementary Materials). For LTO, $a_{LTO} = 0.0043$ Pa · s and $b_{LTO} = 24.66$ ($R^2 = 0.997$); and for LCO, $a_{LCO} = 0.0041$ Pa · s and $b_{LCO} = 24.97$ ($R^2 = 0.998$). The high R^2 correlation coefficients and a parameters being close to the viscosity of the electrolyte (0.0039 Pa · s) indicate this is a good model for LTO and LCO suspensions. The similar values for both a and b in the fits for the measured viscosities of LTO and LCO suspension indicate similar dependence of the viscosity on particle loading and similar interparticle interactions in the suspensions. Both suspensions have high values of parameter b, indicating that the viscosities of both suspensions have strong dependence of particle loading. The parameter b_{LCO} is slightly greater than a_{LTO}; therefore, the viscosities of LCO suspensions are expected to increase at a slightly faster rate than LTO suspensions. Nevertheless, the two suspensions showed very similar exponential increase of viscosities over particle volumetric loading. While higher particle loadings increase the energy density of the electrolytes, the viscosity increases rapidly with the increased loading. This trend opens a new challenging task for increasing the energy density by increasing the loading. Surfactants have previously been reported to help stabilize particulate suspensions and decrease the viscosity [52,53], and future research efforts will be needed on incorporating surfactants and determining the detailed tradeoffs between loading and pumping requirements for various electrochemical cell configurations.

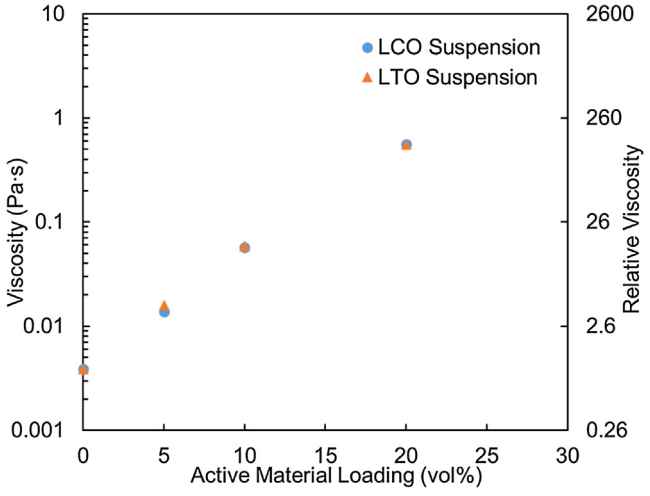

Fig. 3. The viscosities and relative viscosities for the particle-free electrolyte (1.2 M $LiPF_6$ in EC:EMC = 3:7 solvents) and the electrolyte laden with 5, 10, and 20 vol% LCO (blue circle) and LTO (orange triangle) measured at $100\,s^{-1}$.(For interpretation of the references to color in this figure legend, the reader is referred to the web version of this article.)

3.3. LCO Dispersions Half Cell Electrochemical Characterization

Vial cells were used for electrochemical characterization of the LCO dispersed in the electrolyte. As depicted in Fig. 1a, the cathode is the LCO suspension with aluminum wire as the current collector, while a single lithium foil is adopted as the anode and reference electrode. This customized geometry was selected for three reasons. First, the suspension can be easily and continuously agitated to keep the LCO particles in suspension by rotation of the magnetic stirring bar. Second, the distance between the cathode and anode is controllable, reproducible, and kept small to minimize the IR drop. Third, the cell is relatively easy to assemble and disassemble for changing out different dispersion solutions for analysis. Cyclic voltammetry (CV) was first adopted to confirm the potentials of the redox reactions in the LCO dispersion electrolyte. A typical CV scan at 5 mV/s for a 10 vol% LCO suspension is shown in Fig. 4a. The oxidation reaction started at ~3.9 V and the current continued to increase, whereas the reduction curve showed a peak at ~3.8 V. The location of the onset potential for oxidation and peak potential for reduction were consistent with the electrochemical redox potentials for the LCO material in the suspension and indicated that the LCO particles were electrochemically active for lithium extraction/insertion and corresponding cobalt oxidation/reduction in the flowing dispersion [32,38,54]. Note that the cathodic current kept increasing without an obvious peak during the scan. This was because the LCO suspension was being agitated throughout the test and the current response was low, showing no diffusion limitation for the continuous exchange of fresh

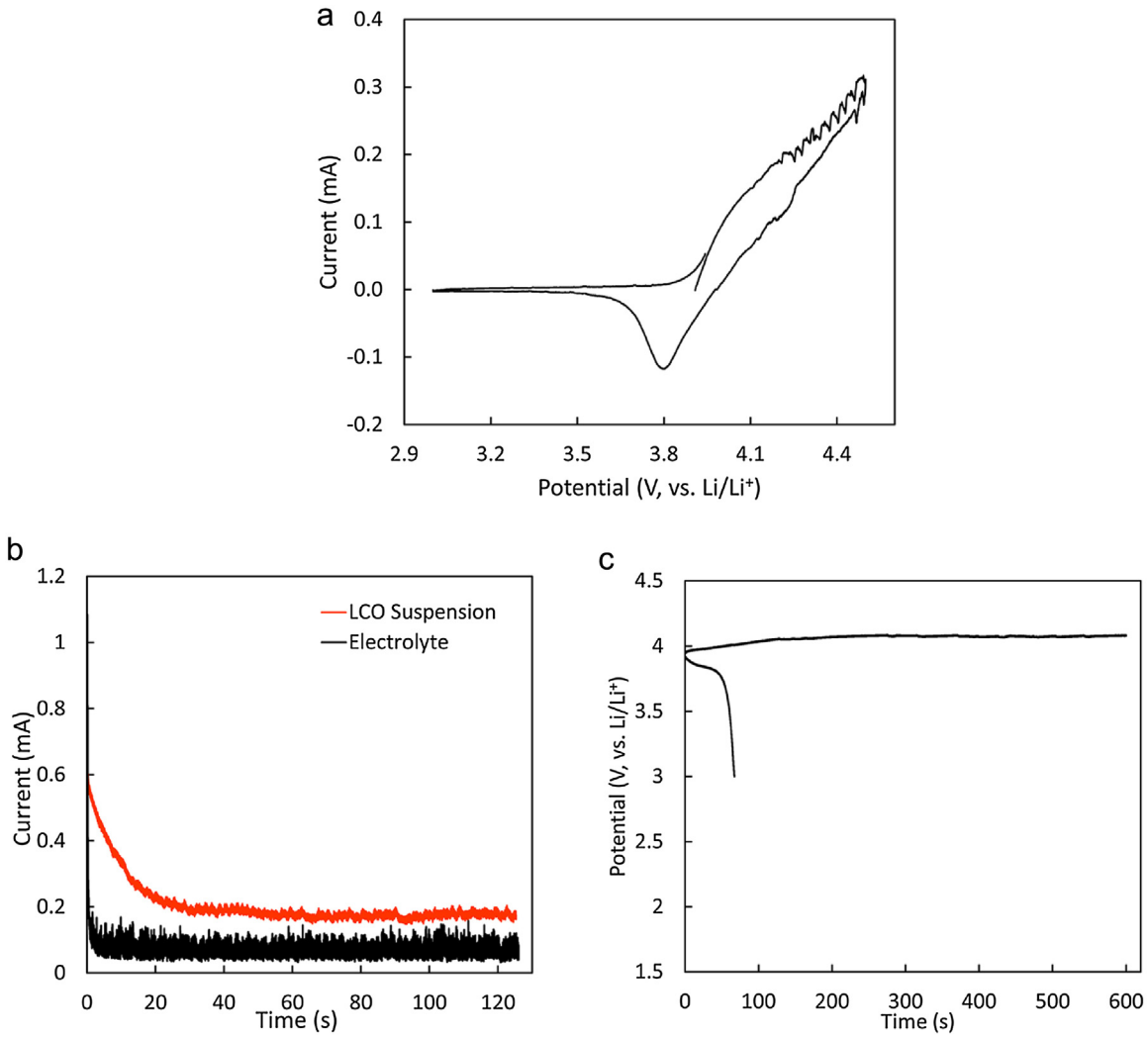

Fig. 4. (a) CV scans at the rate of 5 mV/s between 3.0 and 4.5 V (vs. Li), (b) CA profiles for the control electrolyte (black) and electrolyte with 10 vol% dispersed LCO (red) with applied potential of 4.3 V, and (c) charge (10-minute cutoff time) and discharge curves for the vial cell with an LCO concentration of 10 vol% at a rate of 0.08 mA.(For interpretation of the references to color in this figure legend, the reader is referred to the web version of this article.)

electroactive LCO particles in the flowing environment. However, an anodic peak was clearly observed, which we attribute to be a consequence of the small amount of LCO material that was oxidized during the cathodic scan. Thus, the reduction current was quickly limited by the low concentration of the oxidized LCO and the current decreased quickly as the anodic scan continued down to 3.0 V because very little "charged" LCO was available in the suspension. The CV scan suggests that the electrochemical oxidation of LCO in the suspension was reversible. Also, we note that the oxidation curve was fluctuating at high potentials $> \sim 4.3$ V. We attribute this phenomenon to three factors: first, the inhomogeneity of collision frequencies of LCO particles on the current collector caused current fluctuations throughout the experiments; second, this fluctuation was greater when a higher voltage was applied because of the greater total currents in response to the greater applied potential; third, the electrolyte decomposition and aluminum corrosion also became significant and contributed to the observed current at these high potentials [55–58].

To demonstrate the ability of the LCO suspension to stably undergo charging of the LCO material, a Chronoamperometry (CA) test was conducted at a fixed charge potential of 4.3 V and the results are shown in Fig. 4b. This voltage was chosen for the experiment because it was above the initial redox charging potential of LCO at ~3.9 V (Fig. 2) and below a typical potential where corrosion has been reported to provide significant current for the aluminum current collector in the organic electrolyte [55–58]. A relatively short two-minute test was used because this amount of time was sufficient to provide a stable current signal. The control experiment with electrolyte free of LCO particles had a measured current of 0.068 ± 0.017 mA over the last minute of the test. We attribute the measured current to be primarily the initial background current for electrolyte decomposition and aluminum corrosion in the organic electrolyte [39,41,59,60]. The current measured with the LCO suspension for the last minute of the test was 0.175 ± 0.008 mA, which after adjusting for the current measured for the particle-free electrolyte suggests that ~0.107 mA current was due to the electrochemical oxidation and de-lithiation of the LCO particles in the suspension. The quickly dropping current in the first ~20 seconds of the CA test indicated that extra current was measured initially due to electrochemical double layer formation and possibly a very small amount of LCO particles attached on the aluminum current collector [18,61]. We expect that the stable measured current of the

last minute of the CA test was limited by LCO particle collision frequency, the mass of LCO particles participating in electrochemical oxidation at any given time, and the electronic/ionic conductivity of LCO particles in the suspension [18,20], rather than mass transfer diffusion limitations of lithium ions in the electrolyte [62]. The detailed mechanisms and limitations of the current density are currently under research, but the total mass of active material on average participating in the electrochemical reactions and in contact with the current collector likely plays a major role in the resistance to transferring current in the system [63]. We speculate that the amount of active material participation plays a role because a higher loading of electroactive material per current collector area has previously been reported to result in a lower resistance in coin cell studies with composite electrodes within a broad range of active material loading [64–66]. Previous reports on LTO suspensions also demonstrated that the measured current decreased for decreasing active material loadings [18,67].

A charge/discharge cycling test was performed to demonstrate the electrochemical reversibility of the LCO suspension in a flow battery-type environment. The test was performed with the 10 vol % LCO suspension after the CV and CA test, and the results are shown in Fig. 4c. The suspension was first charged for 10 minutes at a current of 0.08 mA (0.008 mA cm^{-2}) before discharging at the same current. The charge potential quickly reached a plateau at ~4.0 V and remained steady at that potential during the test period. The discharge curve also showed a relatively stable voltage at ~3.8 V. This pair of charge and discharge potentials is consistent with the particle coin cell cycling potential profiles at low depth of charge range shown in Fig. 2b. This not only further confirmed the reversible electrochemical reactions of LCO suspension, but also indicates that the suspension can provide stable power supply from the discharge of LCO particles at a low overpotential. We note that less discharge capacity was achieved relative to the charge capacity (0.013 mAh total charge capacity compared to 0.0015 mAh total discharge capacity resulting in a coulombic efficiency of 11.5%). This was because only a small portion of the LCO had been charged during the 10-minute period (0.013 of the ~800 mAh total available capacity available, or ~0.002% of the total capacity in the suspension). Due to the low concentration, most of the charged particles may not be able to collide with the current collector effectively to deliver capacity during the short discharge period, resulting in a low coulombic efficiency. This cycling behavior is also

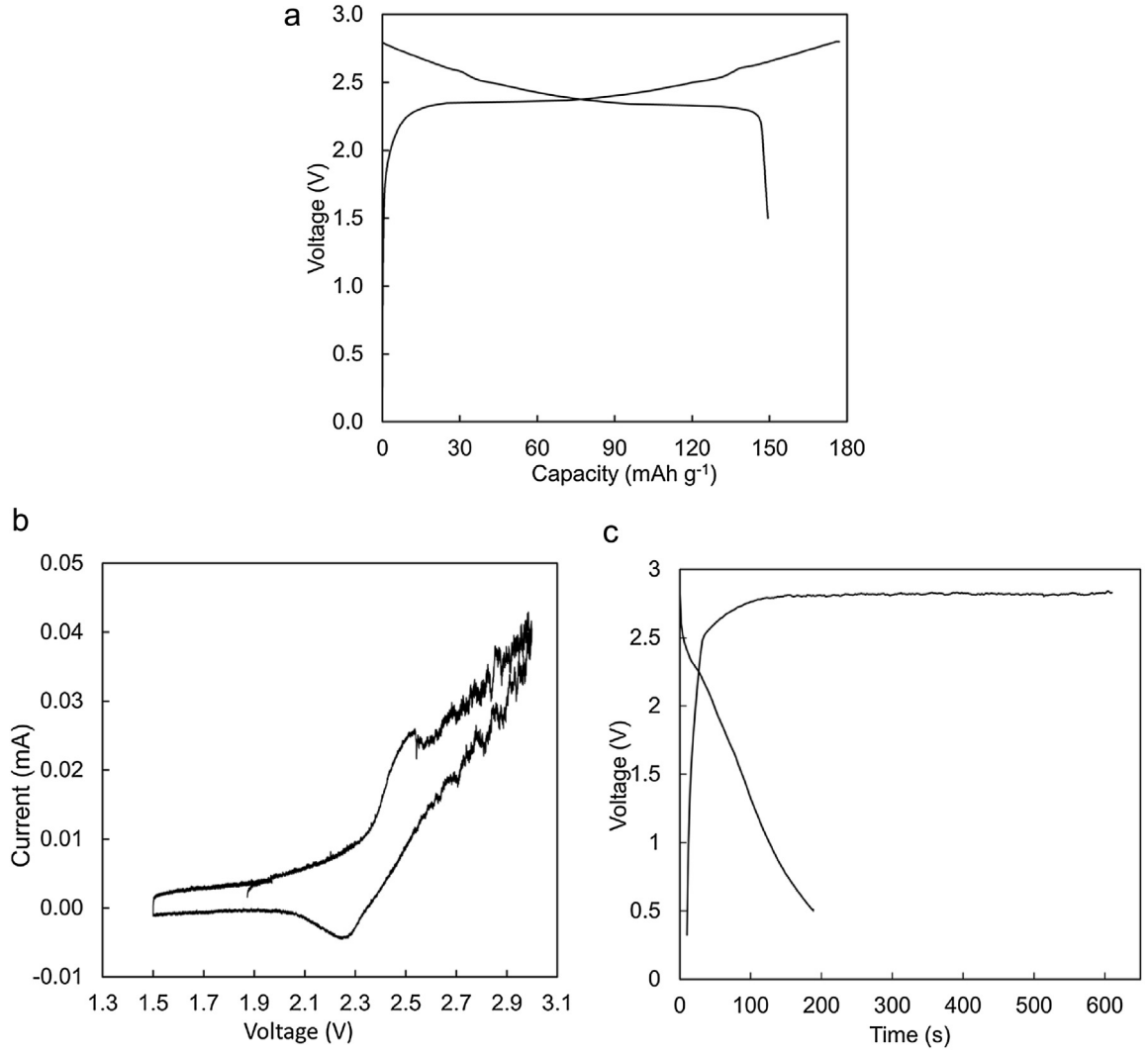

Fig. 5. (a) First charge and discharge cycle of an LTO/LCO conventional coin cell; (b) CV scan at 20 mV s^{-1} between 1.5–3.0 volts (relative to the LTO anolyte) of the full cell containing a 1 vol% LTO anolyte and 0.5 vol% LCO catholyte while stirring at 400 rpm; (c) a constant current charge at 0.02 mA and discharge at 0.001 mA test (cutoff voltages of 0.5 and 3 V) on the same cell. The charge cycle was limited to 10 minutes.

similar to previous reports for LTO suspensions in terms of both voltage profile and coulombic efficiency [18]. We did not perform a full charge and discharge test because this 10-minute test was representative enough to show the cycling reversibility; and full cycling of the suspensions for this dispersion flow battery are impractical with the existing current collector design. Due to the small surface area of the aluminum current collector, only a very small portion of active materials participate in the electrochemical reaction at any given time, while the majority of the particles are suspended in the electrolyte and do not contribute to the measured electrochemical activity. However, all particles will eventually exchange with those participating in electrochemical reactions and hence contribute to the total cell capacity. We estimate that with the current we are able to use for charge/discharge (kept low to avoid large voltage drops) and the total amount of active material in the suspensions, that a full charge and discharge of the LCO suspension would take ~7 months. We are actively investigating methods to increase the current density while avoiding a high viscosity interconnected carbon network, such as modified current collector designs that promote greater average amounts of active material being oxidized/reduced per area of current collector.

3.4. Full Dispersion Flow Cell Electrochemical Characterization

Before constructing an LTO/LCO dispersion full cell with the active materials dispersed in the electrolyte, first a conventional LTO/LCO coin cell was constructed to confirm the expected charge and discharge behavior for the paired materials in a full cell. Fig. 5a shows the first cycle of a LTO/LCO conventional coin cell. The first charge capacity reached 177 mAh g^{-1} with a discharge capacity of 149 mAh g^{-1} (both based on the mass of LCO) for a cell cycled at a rate of 0.1C between the voltage window of 1.5 V to 2.8 V, resulting a coulombic efficiency of 84.4%. The initial capacity of the LTO electrode was approximately double the initial capacity of the LCO electrode to minimize the possibility of lithium deposition during cycling. The charge curve first showed a plateau at ~2.4 V and then slowly increased to the cutoff voltage of 2.8 V. The discharge curve showed a corresponding behavior with voltage slowly decreasing to the ~2.4 V plateau. This was consistent with observations of LTO/LCO cells in the literature [68,69]. Relative to Li/Li^+, LTO has a flat ~1.55 V charge/discharge plateau, while LCO begins charging at 3.95 V and the voltage slowly increases as the extent of delithiation increases [22,28,29,36,37,39,69]. We note that the discharge capacity was slightly lower but close to the LCO half-cell capacity. The discharge capacity being close to that observed for the LCO half-cells was consistent with the high first cycle coulombic efficiency of the LTO material (~0.7%) [18]. However, the full cell charge capacity was slightly lower than the half-cell which we attributed to the relatively low charge cutoff for our LTO/LCO cell. The 2.8 V vs. LTO cutoff (~4.35 V vs. Li/Li^+) in the full cell was ~ 0.15 V lower than the 4.50 V charge cutoff voltage used in the half-cell. Overall, this test confirmed the electrochemical activity for the LTO/LCO full cell and provided expected potentials for electrochemical activity for the experiments with LTO and LCO suspensions.

A dispersed solid LTO/LCO full cell was constructed using the setup illustrated in Fig. 1b and characterized electrochemically with 0.5 vol% LCO suspension as the catholyte and 1 vol% LTO suspension as the anolyte. Relatively low loadings of active materials were used in this cell in order to achieve relatively higher extents of charge in less time. The redox potentials for the LTO and LCO suspensions with lower active material loadings were confirmed to be comparable to the higher loading suspensions. Cyclic voltammetry and galvanostatic charge/discharge testing indicated the same reversible redox reactions for both 0.5 vol% and 10 vol% LCO suspensions (see Supplementary Materials, Figs. S5a-b for 0.5 vol% LCO compared with Figs. 4a,c for the 10 vol% LCO suspension), although the oxidation of LCO in the vial cell is more complex to interpret due to electrolyte decomposition and/or aluminum corrosion. The reversible redox behavior also has been observed to be at similar potentials for LTO suspensions within the range of 0.5 vol% and 20 vol%, as demonstrated in two previous reports [18,67]. Chronopotentiometry results for a 1 vol% LTO suspension (the same loading as used in the LTO/LCO full cell experiment) in a vial cell paired with lithium metal can also be found in Fig. S5c. The 1 vol% LTO suspension reached a plateau of ~1.55 V (vs. Li/Li^+) in less than 3 minutes, and the measured redox potential was consistent with measurements using the same material within a 10 vol% LTO suspension as well as conventional LTO electrodes in coin cells paired with lithium metal. A CV test on the LTO/LCO dispersion full cell was conducted to determine the redox potential of the electrochemical reactions in the full cell and the result is shown in Fig. 5b. The measured current was relatively noisy during the experiment, likely because of the stochastic nature of the particle collisions necessary now at both current collectors to provide the charging current [70]. Due to the agitation and flow profile in the vial, the concentration of active materials was not perfectly homogeneous in the suspension and local collision frequencies of the active material particles on the current collector were likely not constant, i.e. the total mass of active materials that are contributing to the electrochemical reactions are not constant with time. Although the oxidation current increased continuously with the increasing potential in general, the current showed a small peak at 2.52 V and became noisier above this potential. While the currents measured at higher potentials likely had contributions from the corrosion of aluminum wire and electrolyte decomposition [39,41,59,60], the increase in measured current at 2.26 V and the slight peak at 2.52 V (relative to LTO dispersion) were consistent with potentials expected for an LTO/LCO cell. The reduction peak at 2.26 V demonstrated that the redox reactions with the LTO/LCO cell suspensions were reversible. The approximate half-wave value, $E_{1/2}$ is 2.39 V [71]. This is consistent with the average potential at low state of charge in the LCO and LTO coin cell, indicating the source of the redox reaction was the LTO/LCO redox reaction pair. These results are the first demonstration of a reversible lithium-ion solid dispersion electrochemical flow cell, where all of the electrochemical activity is from collisions of lithium-ion active materials with current collectors placed in the anolyte and catholyte.

The oxidation peak was higher than the reduction peak in the CV measurement. This is due to a lower concentration of available active materials during the anodic compared to the cathodic reactions. The original suspension was pure pristine LCO and LTO. All of the LCO particles started in the reduced state and all of the LTO particles started in the oxidized state relative to the electrochemical processes of interest (effectively fully discharged LCO and LTO for full cell purposes). During the discharge sweep of the CV, only a tiny portion active material particles ($< 0.01\%$) had been reacted (delithiated LCO and lithiated LTO) and were available to have the electrochemical reactions reversed. Therefore, the concentration of active particles available for the discharge reactions was very low relative to the original active material concentration.

The LTO/LCO dispersion electrochemical cell was also galvanostatically partially charged and discharged to demonstrate the potential to use the anolyte/catholyte in a flow battery system. Fig. 5c shows a 10-minute charge of the cell at 0.02 mA and subsequent discharge of the cell down to a cutoff voltage of 0.5 V at 0.001 mA. The charge curve quickly reached a stable potential at 2.82 V, which was higher than the redox potential of ~2.4 V as indicated earlier in the CV test. The charging rate of 0.02 mA was

relatively high for this cell configuration and resulted in additional overpotential due to the resistances in the system (charge transfer, diffusion and Ohmic resistance) [61]. On discharge the cell had a small capacity at ~2.2 V and quickly dropped to the lower cutoff voltage. We attribute the low coulombic efficiency (1.58%) to the low concentration of reacted active materials on both electrodes, similar to the explanation of the lower currents measured during the CV anodic sweep. Approaches to increase the participation rate of the active materials and hence faster cell charging are currently under investigation. This is the first report of an electrochemical cell comprised of only lithium-ion battery active material suspensions providing reversible redox couples in an electrochemical flow cell.

4. Conclusion

An LCO suspension dispersed in organic lithium-ion electrolyte was characterized electrochemically as a catholyte for a solid dispersion redox flow couple. A solid dispersion lithium-ion electrochemical flow cell was demonstrated for the first time by using the LCO suspension as a catholyte and pairing it with an LTO suspension anolyte. While the utilization of the active materials in this preliminary system is low, these results demonstrate the feasibility of reversible charge and discharge of a full cell comprised of lithium-ion active materials dispersed in electrolytes. Such a flow cell has a high operating potential relative to existing flow batteries as demonstrated in this manuscript, theoretically high capacity, and the ability to control the viscosity with active material loading. Future research efforts will need to be directed towards improving the current density and coulombic efficiency of the dispersed particle electrolytes.

Acknowledgements

This research was supported by the National Science Foundation through award ECCS-1405134. We also thank Professor David Green at University of Virginia for use of his lab's rheometer.

Appendix A. Supplementary data

Supplementary data associated with this article can be found, in the online version, at http://dx.doi.org/10.1016/j.electacta.2017.01.061.

References

[1] W. Wang, Q. Luo, B. Li, X. Wei, L. Li, Z. Yang, Recent Progress in Redox Flow Battery Research and Development, Advanced Functional Materials 23 (2013) 970–986.
[2] A. Parasuraman, T.M. Lim, C. Menictas, M. Skyllas-Kazacos, Review of material research and development for vanadium redox flow battery applications, Electrochim. Acta 101 (2013) 27–40.
[3] M. Skyllas-Kazacos, M.H. Chakrabarti, S.A. Hajimolana, F.S. Mjalli, M. Saleem, Progress in Flow Battery Research and Development, Journal of the Electrochemical Society 158 (2011) R55–R79.
[4] P. Alotto, M. Guarnieri, F. Moro, Redox flow batteries for the storage of renewable energy: A review, Renewable and Sustainable Energy Reviews 29 (2014) 325–335.
[5] C.P. de Leon, A. Frias-Ferrer, J. Gonzalez-Garcia, D.A. Szanto, F.C. Walsh, Redox flow cells for energy conversion, J. Power Sources 160 (2006) 716–732.
[6] A.Z. Weber, M.M. Mench, J.P. Meyers, P.N. Ross, J.T. Gostick, Q. Liu, Redox flow batteries: a review, Journal of Applied Electrochemistry 41 (2011) 1137–1164.
[7] T. Janoschka, N. Martin, U. Martin, C. Friebe, S. Morgenstern, H. Hiller, M.D. Hager, U.S. Schubert, An aqueous, polymer-based redox-flow battery using non-corrosive, safe, and low-cost materials, Nature 527 (2015) 78–81.
[8] Y.F. Zhao, S.H. Si, L. Wang, P. Tang, H.J. Cao, Electrochemical Behavior of Polyaniline Microparticle Suspension as Flowing Anode for Rechargeable Lead Dioxide Flow Battery, Journal of the Electrochemical Society 161 (2014) A330–A335.
[9] Y.F. Zhao, S.H. Si, L. Wang, C. Liao, P. Tang, H.J. Cao, Electrochemical study on polypyrrole microparticle suspension as flowing anode for manganese dioxide rechargeable flow battery, J. Power Sources 248 (2014) 962–968.
[10] F.Y. Fan, W.H. Woodford, Z. Li, N. Baram, K.C. Smith, A. Helal, G.H. McKinley, W. C. Carter, Y.M. Chiang, Polysulfide flow batteries enabled by percolating nanoscale conductor networks, Nano letters 14 (2014) 2210–2218.
[11] H.D. Pratt, N.S. Hudak, X.K. Fang, T.M. Anderson, A polyoxometalate flow battery, J. Power Sources 236 (2013) 259–264.
[12] A.P. Kaur, N.E. Holubowitch, S. Ergun, C.F. Elliott, S.A. Odom, A Highly Soluble Organic Catholyte for Non-Aqueous Redox Flow Batteries, Energy Technol-Ger 3 (2015) 476–480.
[13] K. Takechi, Y. Kato, Y. Hase, A highly concentrated catholyte based on a solvate ionic liquid for rechargeable flow batteries, Adv Mater 27 (2015) 2501–2506.
[14] W. Wang, L.Y. Li, Z.M. Nie, B.W. Chen, Q.T. Luo, Y.Y. Shao, X.L. Wei, F. Chen, G.G. Xia, Z.G. Yang, A new hybrid redox flow battery with multiple redox couples, J. Power Sources 216 (2012) 99–103.
[15] S.-H. Kang, W. Lu, K.G. Gallagher, S.-H. Park, V.G. Pol, Study of Li1 + x(Mn4/9Co1/9Ni4/9)1-xO2 Cathode Materials for Vehicle Battery Applications, Journal of The Electrochemical Society 158 (2011) A936–A941.
[16] M. Duduta, B. Ho, V.C. Wood, P. Limthongkul, V.E. Brunini, W.C. Carter, Y.M. Chiang, Semi-Solid Lithium Rechargeable Flow Battery, Adv. Energy Mater. 1 (2011) 511–516.
[17] V. Viswanathan, A. Crawford, D. Stephenson, S. Kim, W. Wang, B. Li, G. Coffey, E. Thomsen, G. Graff, P. Balducci, M. Kintner-Meyer, V. Sprenkle, Cost and performance model for redox flow batteries, J. Power Sources 247 (2014) 1040–1051.
[18] Z. Qi, G.M. Koenig, A carbon-free lithium-ion solid dispersion redox couple with low viscosity for redox flow batteries, J. Power Sources 323 (2016) 97–106.
[19] M. Park, X. Zhang, M. Chung, G.B. Less, A.M. Sastry, A review of conduction phenomena in Li-ion batteries, J. Power Sources 195 (2010) 7904–7929.
[20] H. Li, H. Zhou, Enhancing the performances of Li-ion batteries by carbon-coating: present and future, Chem. Commun. (Cambridge, U.K.) 48 (2012) 1201–1217.
[21] W. Lai, C.K. Erdonmez, T.F. Marinis, C.K. Bjune, N.J. Dudney, F. Xu, R. Wartena, Y. M. Chiang, Ultrahigh-energy-density microbatteries enabled by new electrode architecture and micropackaging design, Adv Mater 22 (2010) E139–E144.
[22] J. Kim, O. Kim, C. Park, G. Lee, D. Shin, Electrochemical Properties of Li1 + xCoO2 Synthesized for All-Solid-State Lithium Ion Batteries with Li2S-P2S5 Glass-Ceramics Electrolyte, J. Electrochem. Soc. 162 (2015) A1041–A1045.
[23] M. Otoyama, Y. Ito, A. Hayashi, M. Tatsumisago, Raman imaging for LiCoO2 composite positive electrodes in all-solid-state lithium batteries using Li2S-P2S5 solid electrolytes, J. Power Sources 302 (2016) 419–425.
[24] D. Ensling, G. Cherkashinin, S. Schmid, S. Bhuvaneswari, A. Thissen, W. Jaegermann, Nonrigid Band Behavior of the Electronic Structure of LiCoO2Thin Film during Electrochemical Li Deintercalation, Chemistry of Materials 26 (2014) 3948–3956.
[25] R. Ruffo, F. La Mantia, C. Wessells, R.A. Huggins, Y. Cui, Electrochemical characterization of LiCoO2 as rechargeable electrode in aqueous LiNO3 electrolyte, Solid State Ionics 192 (2011) 289–292.
[26] R.J. Gummow, M.M. Thackeray, Structure and electrochemistry of lithium cobalt oxide synthesised at 400 °C, Material Research Bulletin 27 (1992) 327–337.
[27] M.S. Whittingham, Lithium Batteries and Cathode Materials, Chem Rev 104 (2004) 4271–4301.
[28] W. Tang, L.L. Liu, S. Tian, L. Li, Y.B. Yue, Y.P. Wu, S.Y. Guan, K. Zhu, Nano-LiCoO2 as cathode material of large capacity and high rate capability for aqueous rechargeable lithium batteries, Electrochem. Commun. 12 (2010) 1524–1526.
[29] K.S. Tan, M.V. Reddy, G.V.S. Rao, B. Chowdari, High-performance LiCoO2 by molten salt (LiNO3: LiCl) synthesis for Li-ion batteries, J. Power Sources 147 (2005) 241–248.
[30] A.M. Gaikwad, B.V. Khau, G. Davies, B. Hertzberg, D.A. Steingart, A.C. Arias, A High Areal Capacity Flexible Lithium-Ion Battery with a Strain-Compliant Design, Adv. Energy Mater 5 (2015) 1401389.
[31] F. Rahman, M. Skyllas-Kazacos, Vanadium redox battery: Positive half-cell electrolyte studies, J. Power Sources 189 (2009) 1212–1219.
[32] Z. Qi, G.M. Koenig Jr., High-Performance LiCoO2 Sub-Micrometer Materials from Scalable Microparticle Template Processing, ChemistrySelect 1 (2016) 3992–3999.
[33] S.K. Martha, O. Haik, V. Borgel, E. Zinigrad, I. Exnar, T. Drezen, J.H. Miners, D. Aurbach, Li4Ti5O12/LiMnPO4 Lithium-Ion Battery Systems for Load Leveling Application, Journal of the Electrochemical Society 158 (2011) A790–A797.
[34] V.V. Viswanathan, D. Choi, D. Wang, W. Xu, S. Towne, R.E. Williford, J.-G. Zhang, J. Liu, Z. Yang, Effect of entropy change of lithium intercalation in cathodes and anodes on Li-ion battery thermal management, J. Power Sources 195 (2010) 3720–3729.
[35] A. Burukhin, O. Brylev, P. Hany, B.R. Churagulov, Hydrothermal synthesis of LiCoO(2) for lithium rechargeable batteries, Solid State Ionics 151 (2002) 259–263.
[36] B. Huang, Y.I. Jang, Y.M. Chiang, D.R. Sadoway, Electrochemical evaluation of LiCoO2 synthesized by decomposition and intercalation of hydroxides for lithium-ion battery applications, J Appl Electrochem 28 (1998) 1365–1369.
[37] H.Y. Liang, X.P. Qiu, H.L. Chen, Z.Q. He, W.T. Zhu, L.Q. Chen, Analysis of high rate performance of nanoparticled lithium cobalt oxides prepared in molten KNO3 for rechargeable lithium-ion batteries, Electrochem. Commun. 6 (2004) 789–794.
[38] H. Liang, X. Qiu, S. Zhang, Z. He, W. Zhu, L. Chen, High performance lithium cobalt oxides prepared in molten KCl for rechargeable lithium-ion batteries, Electrochem. Commun. 6 (2004) 505–509.

[39] M.J.K. Reddy, S.H. Ryu, A.M. Shanmugharaj, Synthesis of nanostructured lithium cobalt oxide using cherry blossom leaf templates and its electrochemical performances, Electrochim. Acta 189 (2016) 237–244.
[40] M.B. Pinson, M.Z. Bazant, Theory of SEI Formation in Rechargeable Batteries: Capacity Fade, Accelerated Aging and Lifetime Prediction, Journal of the Electrochemical Society 160 (2012) A243–A250.
[41] K. Xu, Electrolytes and Interphases in Li-Ion Batteries and Beyond, Chem. Rev. (Washington, DC, U.S.) (2014) 11503–11618.
[42] D. Aurbach, Y. Talyosef, B. Markovsky, E. Markevich, E. Zinigrad, L. Asraf, J.S. Gnanaraj, H.J. Kim, Design of electrolyte solutions for Li and Li-ion batteries: a review, Electrochim. Acta 50 (2004) 247–254.
[43] H.F. Wang, Y.I. Jang, B.Y. Huang, D.R. Sadoway, Y.T. Chiang, TEM study of electrochemical cycling-induced damage and disorder in LiCoO2 cathodes for rechargeable lithium batteries, Journal of the Electrochemical Society 146 (1999) 473–480.
[44] T. Ohzuku, A. Ueda, N. Yamamoto, Zero-Strain Insertion Material of Li[Li1/3Ti5/3]O4 for Rechargeable Lithium Cells, J. Electrochem. Soc 142 (1995) 1431–1435.
[45] T. Ohzuku, A. Ueda, Why transition metal (di)oxides are the most attractive materials for batteries, Solid State Ionics 69 (1994) 201–211.
[46] B. Rieger, S.V. Erhard, K. Rumpf, A. Jossen, A New Method to Model the Thickness Change of a Commercial Pouch Cell during Discharge, Journal of The Electrochemical Society 163 (2016) A1566–A1575.
[47] E.V. Timofeeva, W.H. Yu, D.M. France, D. Singh, J.L. Routbort, Base fluid and temperature effects on the heat transfer characteristics of SiC in ethylene glycol/H2O and H2O nanofluids, Journal of Applied Physics 109 (2011) 014914.
[48] E.V. Timofeeva, D.S. Smith, W.H. Yu, D.M. France, D. Singh, J.L. Routbort, Particle size and interfacial effects on thermo-physical and heat transfer characteristics of water-based alpha-SiC nanofluids, Nanotechnology 21 (2010) 215703.
[49] C.T. Nguyen, F. Desgranges, G. Roy, N. Galanis, T. Mare, S. Boucher, H.A. Mintsa, Temperature and particle-size dependent viscosity data for water-based nanofluids-Hysteresis phenomenon, Int J Heat Fluid Fl 28 (2007) 1492–1506.
[50] W.J. Tseng, K.-C. Lin, Rheology and colloidal structure of aqueous TiO2 nanoparticle suspensions, Materials Science and Engineering: A 355 (2003) 186–192.
[51] J. Mewis, N.J. Wagner, Colloidal suspension rheology, Cambridge University Press, Cambridge, UK, New York, 2012.
[52] L. Madec, M. Youssry, M. Cerbelaud, P. Soudan, D. Guyomard, B. Lestriez, Surfactant for Enhanced Rheological, Electrical, and Electrochemical Performance of Suspensions for Semisolid Redox Flow Batteries and Supercapacitors, ChemPlusChem 80 (2015) 396–401.
[53] S. Sen, V. Govindarajan, C.J. Pelliccione, J. Wang, D.J. Miller, E.V. Timofeeva, Surface Modification Approach to TiO2 Nanofluids with High Particle Concentration, Low Viscosity, and Electrochemical Activity, ACS applied materials & interfaces 7 (2015) 20538–20547.
[54] M. Okubo, E. Hosono, J. Kim, M. Enomoto, N. Kojima, T. Kudo, H. Zhou, I. Honma, Nanosize Effect on High-Rate Li-Ion Intercalation in LiCoO2 Electrode, J. Am. Chem. Soc. 129 (2007) 7444–7452.
[55] S.S. Zhang, T.R. Jow, Aluminum corrosion in electrolyte of Li-ion battery, J. Power Sources 109 (2002) 458–464.
[56] B. Markovsky, F. Amalraj, H.E. Gottlieb, Y. Gofer, S.K. Martha, D. Aurbach, On the Electrochemical Behavior of Aluminum Electrodes in Nonaqueous Electrolyte Solutions of Lithium Salts, Journal of The Electrochemical Society 157 (2010) A423–A429.
[57] X. Zhang, T.M. Devine, Identity of Passive Film Formed on Aluminum in Li-Ion Battery Electrolytes with LiPF[sub 6], Journal of The Electrochemical Society 153 (2006) B344–B351.
[58] M. Morita, T. Shibata, N. Yoshimoto, M. Ishikawa, Anodic behavior of aluminum in organic solutions with different electrolytic salts for lithium ion batteries, Electrochemica Acta 47 (2002) 2787–2793.
[59] A.S. Arico, P. Bruce, B. Scrosati, J.M. Tarascon, W. Van Schalkwijk, Nanostructured materials for advanced energy conversion and storage devices, Nat. Mater. 4 (2005) 366–377.
[60] P. Handel, G. Fauler, K. Kapper, M. Schmuck, C. Stangl, R. Fischer, F. Uhlig, S. Koller, Thermal aging of electrolytes used in lithium-ion batteries – An investigation of the impact of protic impurities and different housing materials, J. Power Sources 267 (2014) 255–259.
[61] C.H. Hamann, A. Hamnett, W. Vielstich, Electrochemistry, 2 ed., Wiley-VCH, 2007.
[62] J.K. Ko, K.M. Wiaderek, N. Pereira, T.L. Kinnibrugh, J.R. Kim, P.J. Chupas, K.W. Chapman, G.G. Amatucci, Transport, phase reactions, and hysteresis of iron fluoride and oxyfluoride conversion electrode materials for lithium batteries, ACS applied materials & interfaces 6 (2014) 10858–10869.
[63] M. Gaberscek, R. Dominko, J. Jamnik, Is small particle size more important than carbon coating? An example study on LiFePO4 cathodes, Electrochem. Commun. 9 (2007) 2778–2783.
[64] M. Gaberscek, A Method for Fast Estimation of the Rate-Limiting Step in Lithium-Ion Batteries, Acta Chim. Slov 61 (2014) 480–487.
[65] K.G. Gallagher, P.A. Nelson, D.W. Dees, Simplified calculation of the area specific impedance for battery design, J. Power Sources 196 (2011) 2289–2297.
[66] D. Dees, E. Gunen, D. Abraham, A. Jansen, J. Prakash, Electrochemical Modeling of Lithium-Ion Positive Electrodes during Hybrid Pulse Power Characterization Tests, Journal of The Electrochemical Society 155 (2008) A603–A613.
[67] Z. Qi, G.M. Koenig Jr., Electrochemical Evaluation of Suspensions of Lithium-Ion Battery Active Materials as an Indicator of Rate Capability, Journal of The Electrochemical Society 164 (2017) A151–A155.
[68] N. Aliahmad, M. Agarwal, S. Shrestha, K. Varahramyan, Paper-Based Lithium-Ion Batteries Using Carbon Nanotube-Coated Wood Microfibers, IEEE Transactions on Nanotechnology 12 (2013) 408–412.
[69] N. Takami, H. Inagaki, T. Kishi, Y. Harada, Y. Fujita, K. Hoshina, Electrochemical Kinetics and Safety of 2-Volt Class Li-Ion Battery System Using Lithium Titanium Oxide Anode, Journal of The Electrochemical Society 156 (2009) A128–A132.
[70] A. Fernando, S. Parajuli, M.A. Alpuche-Aviles, Observation of individual semiconducting nanoparticle collisions by stochastic photoelectrochemical currents, J Am Chem Soc 135 (2013) 10894–10897.
[71] A.B. Bocarsly, CV overview from Wiley Characterization of Materials, in: E.N. Kaufmann (Ed.), Characterization of Materials, John Wiley & Sons, 2012.